ORIGINAL PAPER

The multiscale model is illustrated with the computation of the fracture properties of high strength alloys (HSA), whose microstructure consists of population of inclusions at two distinct length scales, embedded in a metallic matrix. The study of the fracture of those materials has been an active field of research for decades and many aspects of its underlying mechanisms have been addressed in the literature [2, 6, 7, 9,

Table 1 Material constants of HSA for steel matrix, TiN and TiC particles

(GPa)	1.7
(GPa)	0.6
´ (GPa)	1.0
(GPa)	4.1
ʹ ´	0.01
ʹ	0.02

scales. On the one hand, the desirable population of second-

Fig. 1 K-dominant region and zone of microstructure damage in a fracture specimen. Process zone model showing the full computational domain for the multiscale process zone model and a zoom of the FEM description around the crack tip
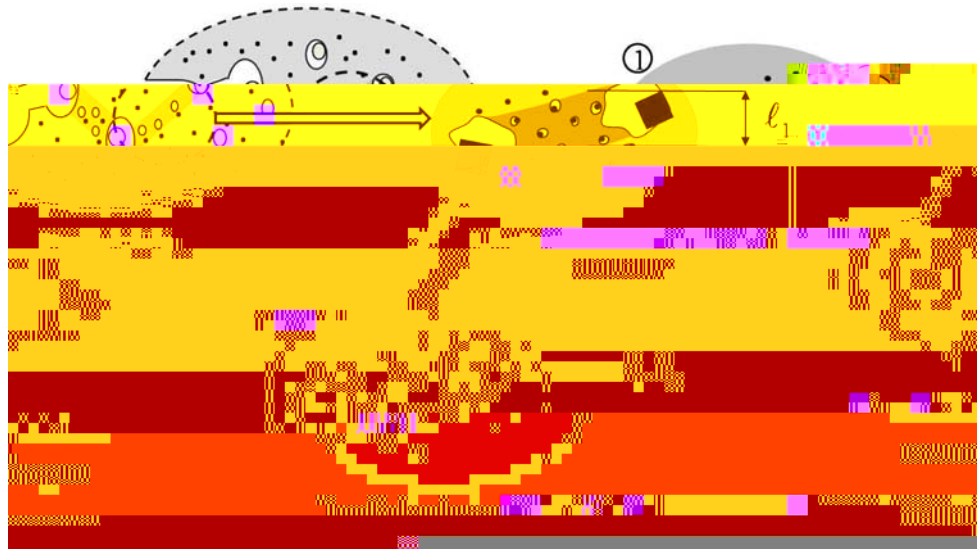
3.1 Multiscale micromorphic model for HSA

Continuum formulations of the strain softening and localization in solids are known to be an issue since the conventional continuum theory does not possess a length-scale in this formulation. This usually leads to a localization region that is not defined, leading to an inadequate estimation of the material behavior after the onset of strain softening. Alternative strategies thus consist in introducing a length-scale into the continuum theory through the incorporation of a second displacement gradient into the expression of the internal energy of the solid. This concept led to micromorphic and strain gradient theories, which possess an intrinsic length scale characterizing the localization region. This paper is concerned with a hierarchical material (HSA), for which localization and failure occurs at several length-scales which can be modeled with the multiscale micromorphic framework developed by Vernerey et al. [30]. Next, we present the model for the failure of HSA, for which localization involves two characteristic length scales associated with the size of primary and secondary inclusions.

The multiscale model for the failure of HSA is based on the multiscale decomposition of the microstructure according to three averaging domains $\bar{}$, ^{1} and ^{2} that can be thought of as representative volume element for the entire microstructure, the material consisting of secondary particles only and the matrix material, respectively (Fig. 2). Based on this decomposition, we introduce three deformation measures as average velocity gradients into each domain: the macro-velocity gradient $\mathbf{L}$ (averaged in $\bar{}$), the micro-velocity $\mathbf{L}^1$ (averaged in ^{1}), and submicro-velocity gradient $\mathbf{L}^2$ (averaged in ^{2}). For further details regarding kinematics, the reader is referred to Vernerey et al. [30].
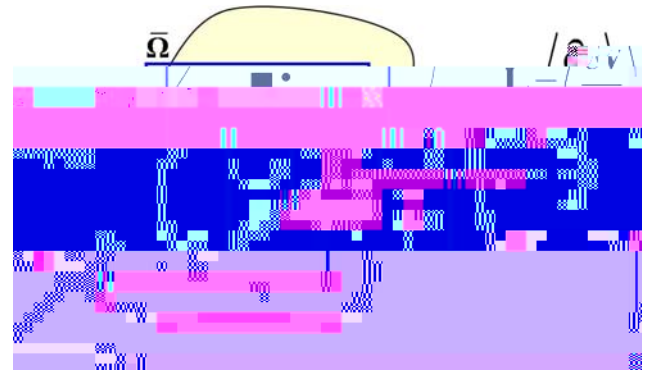
Fig. 2 Proposed multiscale framework for the modeling of HSA. The ___ represent the primary particles and the ___ represent the secondary particles

The expression of internal energy of the multiscale continuum can then be introduced. Only including the effect of stretches at microscale, the internal energy may be written in terms of the symmetric counterparts $\mathbf{D}^1$ and $\mathbf{D}^2$ of the micro-velocity gradients

$\overline{\boldsymbol{\beta}}^2$ and $\overline{\overline{\boldsymbol{\beta}}}^2$ are the submicro-stress and submicroscopic stress couples. A physical interpretation of the various terms can be given as follows. The quantity $\mathbf{D}^1 - \mathbf{D}$

In this work, the above equation is solved with an explicit scheme, such as that addressed in Vernerey et al. [30]. The solution is computed with an explicit dynamic scheme in quasi-static conditions. This is ensured by enforcing a very slow loading rate compared to the speed of elastic waves. The implementation of the nonlinear constitutive relation follows from a semi-implicit backward Euler scheme introduced in Belytschko et al. [3].

3.3 A multiscale damage model for HSA

As depicted in Fig. 1, the failure of HSA is deeharaininThe

evolution of the macro-stress and plastic strains and therefore represents the macroscopic plastic flow derived within the hierarchical methodology. The constitutive relation at the macro-scale:

$$\sigma = \left(\frac{\text{eq}}{\text{}}\right)^2 - 1 + 2\,_1\left(\text{ }+\text{ }\right.$$
$$\times \cosh\left(\frac{3\;2}{2\text{ }}\right) - \,_3$$

Fig. 4 Nucleation strain as a function of the strain hardening parameter for different debonding peak stress at the Fe–TiN interface
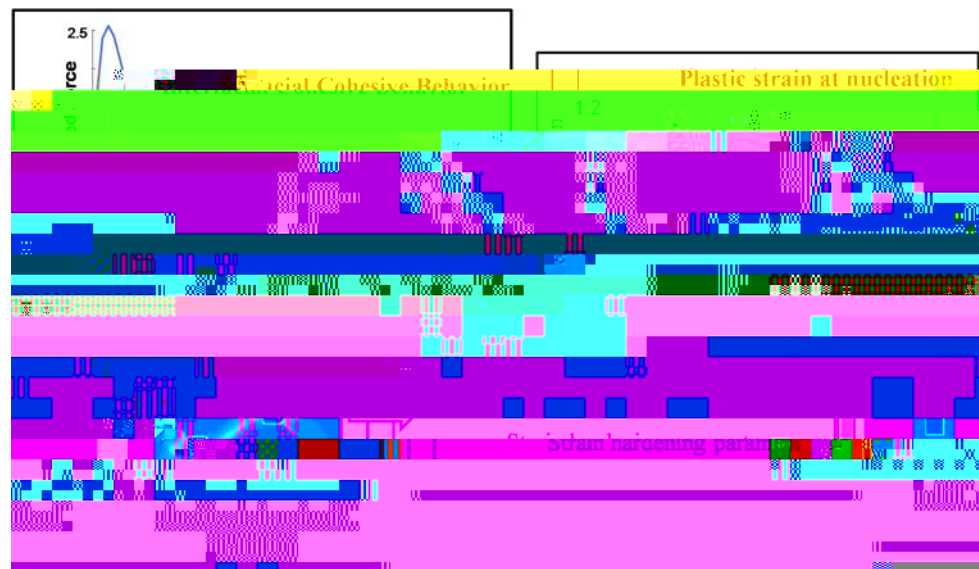
stress. Performing the analysis for different strain hardening parameters   and debonding stress   , a relationship may be derived (as shown in Fig. 4) and used in the constitutive relation described in the previous section. Generally, our simulations show that the nucleation plastic strain decreases with increasing h and increasing   (Fig. 4). This result can be explained by the fact that when the hardening is increased, the stress level at the interface particle/matrix increases at a constant level of average plastic strain. This implies that the harder the matrix material, the earlier the void nucleation.

4 Application to the computation of fracture toughness

In this study, we define the fracture toughness   as the stress intensity factor at which crack growth becomes unstable. This value is determined by plotting the stress intensity factor as a function of the crack opening displacement (COD). The value of   is reached when the slope of the curve changes abruptly as shown in Fig. 5.

4.1 Analysis

The numerical computation of fracture toughness is per-

Fig. 5 Comparison of effective plastic strains for the classical (one-scale) continuum and the three-scale continuum
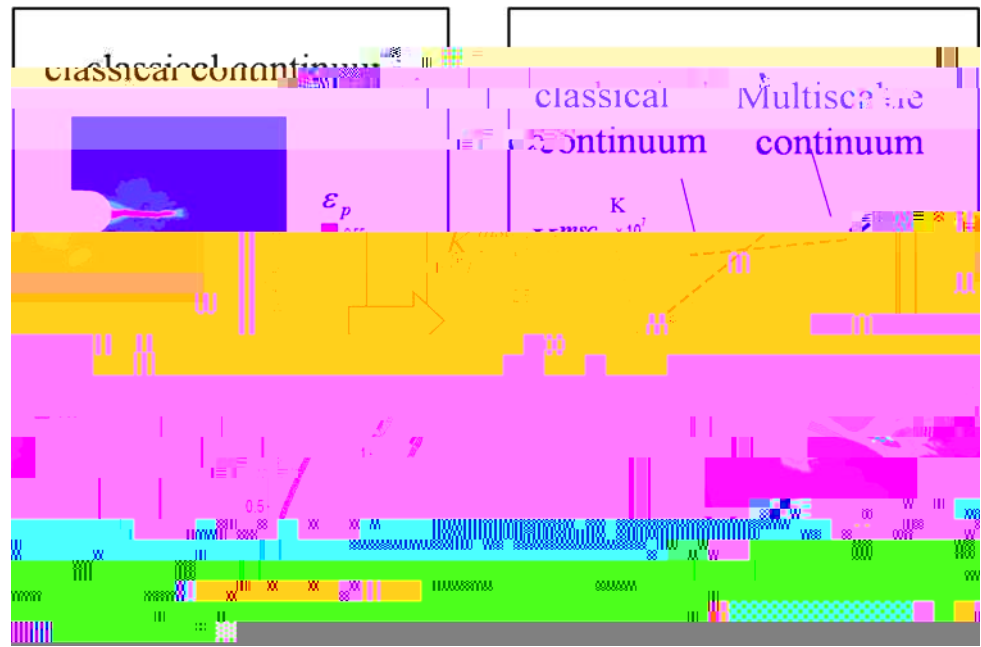
mined by the element size. This non-physical behavior has the effect of underestimating the energy release rate necessary for crack advance and therefore the fracture toughness ^{cc}. On the other hand, with the multiscale technique, the localization region accounts for length scales associated with both primary and secondary particles. Because it accounts for the correct size of the damage region, the multiscale
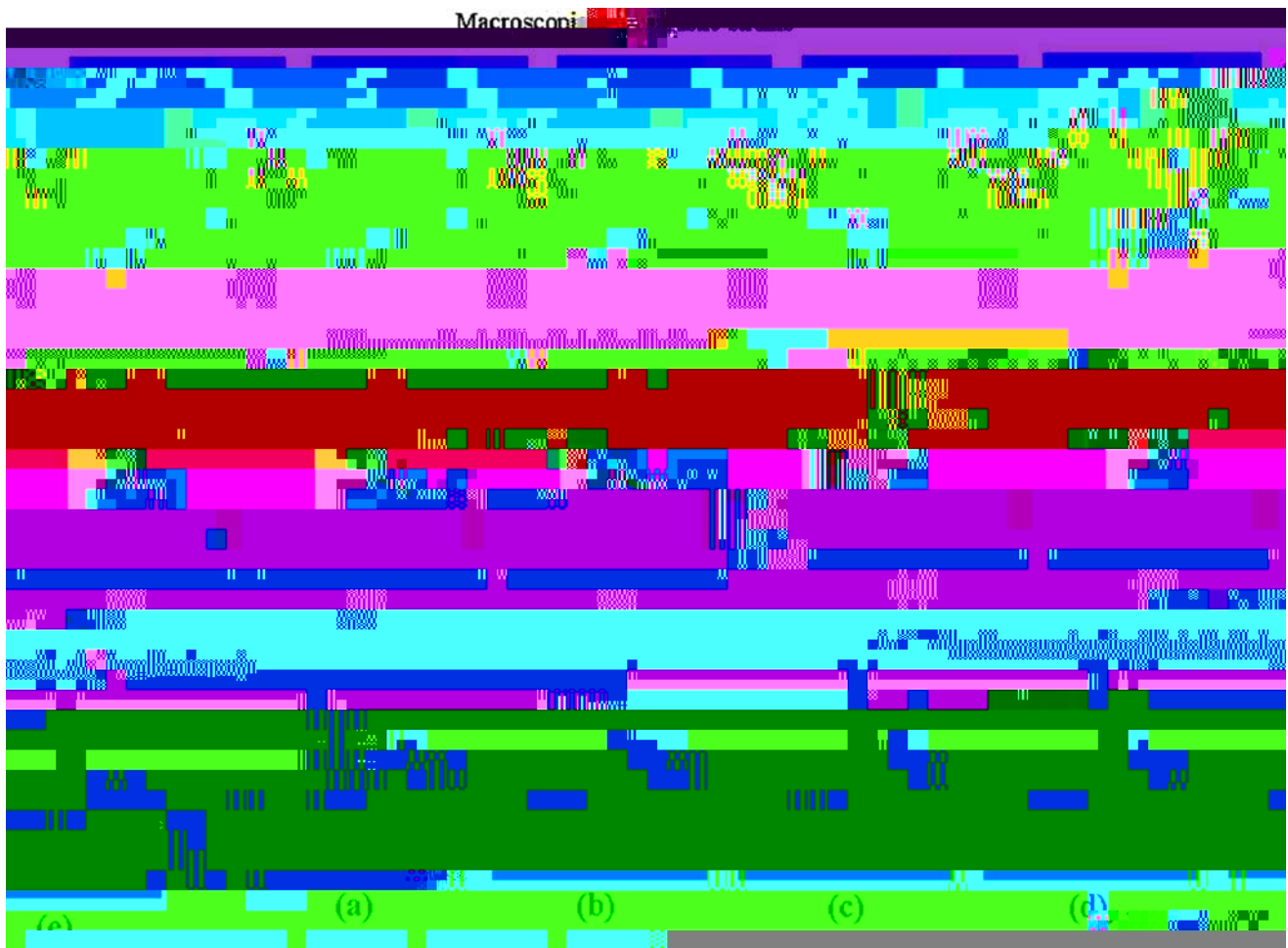
Fig. 6 Evolution of the contours of plastic strains at different scales

The present work aims at providing a relationship between

Fig. 7 Evolution of the contours of tensile stress at different scales
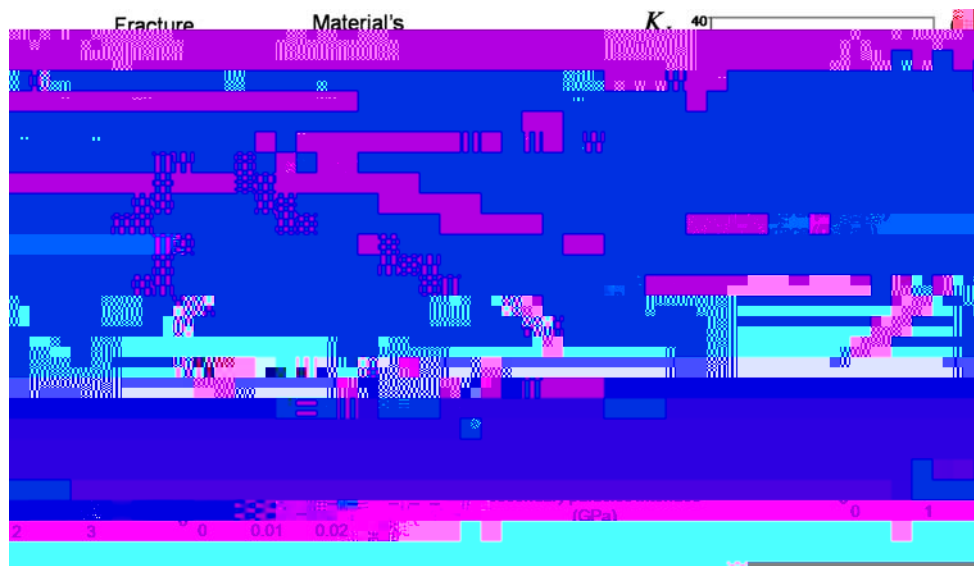
Fig. 8 Variation of fracture toughness as a function of some material key parameters

Figure 8a depicts the variation of fracture toughness with strength, given by the hardening parameter of the matrix material. We observe decreasing fracture toughness with increasing strength that is consistent with experimental observations. This can be explained by the fact that increasing the hardening of the matrix has the effect of precipitating the nucleation of voids by meeting the debonding stress at the particle/matrix interface early in the deformation history. Figure 8d gives the relationship between fracture toughness and debonding peak stress ´ of the interface Fe–TiN of the primary particles. We observe a very steep increase of fracture toughness with ´. The effect of the decohesion stress at the secondary particle–matrix interface on the fracture toughness is not as significant as the effect of ´ as shown in Fig. 8c. This trend can be interpreted as follows. After the nucleation of voids from primary particles, stresses and strains become concentrated in the ligament between larger voids. In other words, a small variation in the stress state at the macroscopic level results in a significant variation locally. Consequently, the debonding peak stress can be reached at a relatively low level of macroscopic stress (or strain) and the influence of the debonding stress is lessened. Figure 8b shows the effect of the volume fraction of primary particles on . As expected, the fracture toughness increases with decreasing particle volume fraction. This can be explained by the fact that at low volume fraction, voids need to grow independently for a long time before reaching the void sheet driven coalescence criterion.

The main trends can be summarized as follows:

– When strength increases, toughness decreases
– The volume fraction of primary particles and the debonding stress are critical parameters to the design of fracture toughness, as they are the first initiator of crack growth.
– The debonding stress is relatively important as large nucleation stress at secondary particles impedes crack growth after nucleation of large voids.

11. Li S, Liu WK (2004) Meshfree particle methods. Springer, Heidelberg, p 502
12. Liu WK, McVeigh C (2008) Predictive multiscale theory for design of heterogeneous materials. Comput Mech 42(2):147–170
13. Liu WK, Jun S, Zhang YF (1995a) Reproducing kernel particle methods. Int J Numer Methods Fluids 20:1081–1106
14. Liu WK, Jun S, Li S, Adee J, Belytschko T (1995b) Reproducing kernel particle methods for structural dynamics. Int J Numer Methods Eng 38:1655–1679
15. Liu WK, Karpov EG, Zhang S, Park HS (2004) An introduction to computational nanomechanics and materials. Comput Methods Appl Mech Eng 193:1529–1578
16. Liu WK, Karpov EG, Parks HS (2006) Nano mechanics and materials, theory, multiscale, methods and applications. Wiley, New York
17. McVeigh C, Liu WK (2008a) Multiresolution modeling of ductile reinforced brittle composites. J Mech Phys Solids. doi:10.1016/j.jmps.2008.10.015
18. McVeigh C, Liu WK (2008b) Linking microstructure and properties through a predictive multiresolution continuum. Comput Methods Appl Mech Eng 197:3268–3290
19. McVeigh C, Vernerey F, Liu WK, Brinson LC (2006) Multiresolution analysis for material design. Comput Methods Appl Mech Eng 95:37–40, 5053–5076
20. McVeigh C, Vernerey F, Liu WK, Moran B (2007) An interactive microvoid shear localization mechanism in high strength steels. J Mech Phys Solids 55:2, 225–244
21. Needleman A, Tvergaard V (1984) An analysis of ductile rupture in notched bars. J Mech Phys Solids 32:461–490
22. Needleman A, Tvergaard V (1987) An analysis of ductile rupture modes at a crack tip. J Mech Phys Solids 35(2):151–183
23. Needleman A, Tvergaard V (1998) Dynamic crack growth in a nonlocal progressively cavitating solid. Eur J Mech A/Solids 17:421–438
24. Pardoen T, Hutchinson JW (2003) Micromechanics-based model for trends in toughness of ductile metals. Acta Mater 51(1):133–148